

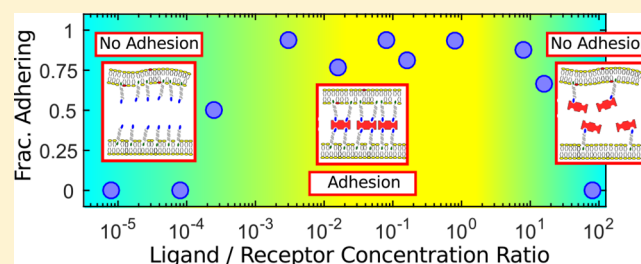
Membrane Adhesion through Bridging by Multimeric Ligands

Omar A. Amjad,[†] Bortolo M. Moggetti,^{‡,ib} Pietro Cicuta,^{*,†,ib} and Lorenzo Di Michele^{*,†,ib}

[†]Biological and Soft Systems, Cavendish Laboratory, University of Cambridge, JJ Thomson Avenue, Cambridge CB3 0HE, United Kingdom

[‡]Université libre de Bruxelles (ULB), Interdisciplinary Center for Nonlinear Phenomena and Complex Systems, Campus Plaine, CP 231, Blvd. du Triomphe, B-1050 Brussels, Belgium

ABSTRACT: Ligand/receptor multivalent interactions have been exploited to drive self-assembly of nanoparticles, hard colloids, and, more recently, compliant units including emulsion droplets and lipid vesicles. In deformable liposomes, formation of links between two membranes produces morphological changes depending on the amount of ligands in the environment. Here, we study a proof-of-concept biosensing system in which single lipid vesicles adhere to a flat supported lipid bilayer, both decorated with membrane-anchored biotinylated receptors. Adhesion is driven by multivalent streptavidin (SA) ligands forming bridges between the vesicles and the supported bilayer. Upon changing the concentration of ligands, we characterize the morphological and mechanical changes of the vesicles, including the formation of a stable adhesion patch, membrane tension, and the kinetics of bridge rupture/formation. We observe vesicle binding only within a specific range of ligand concentrations: adhesion does not occur if the amount of SA is either too low or too high. A theoretical model is presented, elucidating the mechanism underlying this observation, particularly, the role of SA multivalency in determining the onset of adhesion. We elaborate on how the behavior of membranes studied here could be exploited in next-generation (bio)molecular analytical devices.



1. INTRODUCTION

Ligand–receptor multivalent interactions are a powerful tool to drive the self-assembly of artificial Brownian objects and build materials whose local structure would be hard to replicate with top–down manufacturing approaches.^{1–5} Advances in this area benefit from the use of synthetic DNA tethers, whose selective and reversible binding enables a fine control over the resultant multivalent interactions.^{6,7} Such self-assembled phases have applications in molecular diagnostics,⁸ photonics,⁹ and potential nonbiological self-replicating systems.¹⁰ Despite the remarkable control over the structure of these materials, examples of phases exhibiting morphological response to external stimuli are limited, and often rely on precisely engineered reactions between competing linkages that can be achieved only using synthetic DNA tethers, and are hardly applicable with naturally occurring linkers.^{11–13}

However, when the Brownian particles become sufficiently soft, as for the case of emulsion droplets and particularly lipid vesicles,^{14–24} strong enough multivalent interactions can cause significant deformation. As a consequence, the morphology of the self-assembled soft phases can respond dramatically to small changes in the adhesion strength¹⁶ or the stiffness of the particles.¹⁷ Such effects are independent of the details of the ligands and can therefore be seen as a general means of sensing environmental changes. Large morphological variations allow for a specific and strong (nonlinear) amplification of external signals, at the same time enabling their transduction into an easily detectable response—these are major advantages in

analytical sensing. Recent studies have demonstrated a pronounced response to temperature changes in the morphology of DNA-tethered giant unilamellar vesicles (GUVs) and thereby in the porosity vesicle networks.^{16,17} More specifically, structural change in these tissues results in a negative thermal expansion.¹⁷ Such a response emerges from the interplay between the thermal expansion of the surface area of GUVs and the rearrangement of the mobile tethers. Furthermore, the study of the physical properties of lipid-based self-assembled systems is of particular interest owing to their analogy with biological cells. Thus, they can provide a model to study cell and tissue morphology and rheology.¹⁹ Additionally, such works can have implications on the study of compartmentalization and therefore application to the fields of synthetic biology, nanoreactors, nanofiltration, and drug delivery.^{25–27} Specifically, multiple liposomes can be held together by linkers to form multicompartments assemblies. In these systems, engineered linkers can be used to change the morphology of the assembly and/or the distance between the lipid bilayers. If the agents (chemical or biological) in different compartments are to interact via the permeation of species across these bilayers, such morphological changes can serve as a means of controlling interactions. Furthermore, DNA linkers can be used to induce

Received: October 10, 2016

Revised: December 30, 2016

Published: January 10, 2017

fusion between bilayers,^{28,29} effectively merging different compartments.

Having highlighted the responsiveness of networks of tethered GUVs to temperature changes^{16,17} and laid down the foundational theory of such systems,^{16,17,30,31} in this paper we test the response of adhering GUVs to changes in the concentration of free linkers in solution that mediate the adhesion, thus exploring the potential for biosensing. In view of their well-understood interactions, we choose to functionalize the membranes with biotin “receptors”, bridged by tetravalent streptavidin (SA) “ligands”. To unambiguously assess the response to changes in SA concentration, we consider a simplified architecture in which isolated GUVs adhere to large supported lipid bilayers (SLBs) and measure morphological, mechanical, and kinetic features related to adhesion and deformation. In particular, the probability of GUVs forming a stable adhesion *patch* with the SLB and the resultant membrane tension are measured. Bond lifetime is assessed through fluorescence recovery after photobleaching (FRAP). We propose a simple statistical-mechanical model capable of capturing the experimental phenomenology. Specifically, we demonstrate that entropic contributions derived from the tetrameric nature of SA ligands play a crucial role in determining the onset of adhesion upon increasing the ligand concentration and the trend observed in the bond breakup kinetics.

Avidin–biotin interactions were previously adopted to study the adhesion of colloidal units including emulsion droplets and particularly lipid vesicles, starting with the seminal works of Zasadzinski and co-workers, who observed an assembly of small liposomes mediated by SA bridges³² and the formation of compartmentalized liposomes.³³ A variety of properties of such systems have been elucidated. The association rates of ligand–receptor pairs have been shown to decrease in vesicles with increased membrane tension in the work of Bihl et al.³⁴ An increase in the concentration of polymer brushes used to modulate the nonspecific GUV adhesion slowed down the association rates.³⁴ The diffusion rates of both lipids and biotin–avidin complexes have been shown to decrease with an increasing receptor concentration, owing to molecular crowding and membrane viscosity.³⁵ Furthermore, the morphology, formation kinetics, and overall binding strength of adhesive patches have been investigated in systems similar to the one proposed here.^{36–39} Relevant research has been carried out on networks of soft objects assembled through avidin–biotin linkers: Pontani et al. showed that in a densely packed network of emulsion droplets mimicking biological tissues, droplet adhesion strengthens with increasing external pressure.¹⁴ As yet, however, a detailed characterization on the dependency of the adhesion behavior on linker concentration, highlighting the effect of SA multivalency, has not been reported.

The sensitivity of GUV adhesion to ligand concentration can be exploited to design (bio)molecular detection devices featuring packings of receptor-decorated GUVs that sharply change their adhesion probability. Patch formation can then be detected optically or through electrical measurements following the change in the porosity of packings and thereby its resistance to ionic current.

2. EXPERIMENTAL SECTION

2.1. Experimental Design. A schematic of the experimental system is sketched in Figure 1a. Following ref 16, we consider isolated GUVs adhering to an SLB. Compared with the study of GUV–GUV

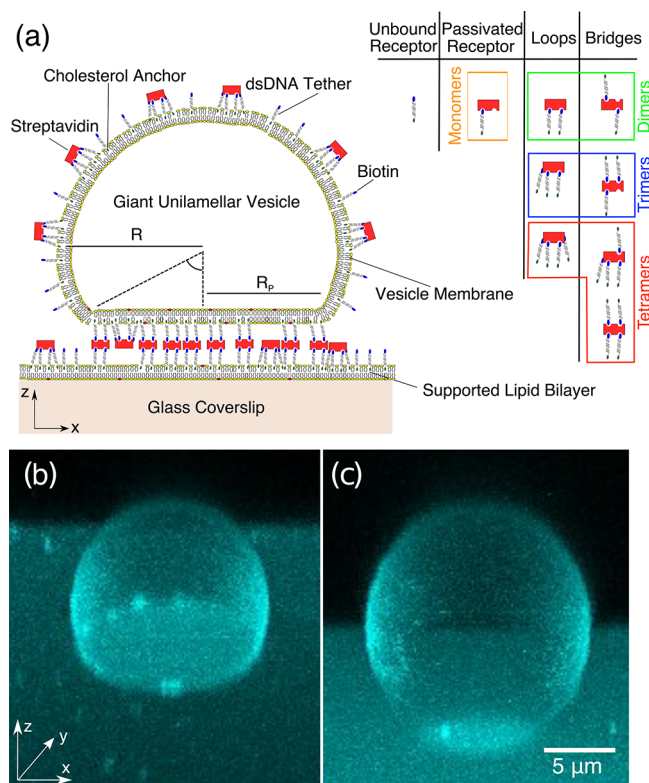


Figure 1. Experimental system. (a) Schematic vertical cross section of a GUV adhering to an SLB. Adhesion is mediated by intermembrane bonds formed by tetravalent SA molecules connecting multiple membrane-anchored DNA–biotin receptors. Various multimeric ligand–receptor complexes are shown in the top-right corner. (b) Confocal 3D reconstructions of a GUV adhering to an SLB, as acquired by imaging fluorescently labeled lipids. (c) Confocal 3D reconstruction of a non-adhering GUV.

interactions, this study with its simplified geometry enables an accurate characterization of the membrane tension of the GUVs and morphological changes. At the same time, the underlying physical mechanisms of GUV–SLB and GUV–GUV adhesions are largely shared.^{16,17}

Both GUVs and SLBs are functionalized with cholesterol-anchored double-stranded DNA (dsDNA) constructs. However, interactions are not mediated by DNA overhangs. Instead, dsDNA receptors are tipped by a biotin molecule, and SA molecules dispersed in solution act as multivalent ligands. SA is a tetrameric protein that provides four biotin-binding sites, one pair on either side of the molecule.⁴⁰ Therefore, the protein can connect multiple receptors and create molecular *bridges* between GUVs and SLBs, driving adhesion. Likewise, complexes in which a single SA connects multiple receptors bound to the same membrane are possible, indicated as *loops* (see Figure 1a). SA does not affect the stability of the vesicle, making it ideally suited for our proof-of-principle experiments.⁴⁰

One may argue that simple biotin-functionalized lipids could have been used instead of biotin-tipped DNA tethers, as previously adopted by several authors.^{32,33} However, our design choice enables two key functions specifically fulfilled by the dsDNA spacers. First, they provide a steric repulsion between bilayers, stopping the membranes from getting into close contact and thus adhering through nonspecific forces (e.g., van der Waals) or even undergoing fusion. We demonstrated in a recent publication how these rigid spacers keep approaching bilayers at distances $>L$, where $L \approx 10$ nm is the length of the dsDNA.¹⁷ Second, in the absence of dsDNA spacers, geometrical constraints due to the spatial arrangement of the binding sites on the bulky SA ligands would affect the formation of certain types of loops, as further discussed below. Long spacers relax these constraints.

2.2. GUV Preparation. GUVs are prepared according to the protocol in ref 17. Briefly, 1,2-dioleoyl-*sn*-glycero-3-phosphocholine (DOPC, Avanti Polar Lipids) and fluorescent Oregon Green 1,2-dihexadecanoyl-*sn*-glycero-3-phosphoethanolamine (DHPE, Thermo Fisher) are dissolved in chloroform in a 99.3:0.7 molar ratio and overall concentration of 3.57 mg mL⁻¹. An indium tin oxide-coated microscope slide is spin-coated on its conductive side with 160 μ L of the lipid solution for 2 min to create a uniform film. The lipid-coated slide is dried in a vacuum desiccator for 1 h. The dried lipid-coated slide and a clean non-lipid-coated slide are arranged together to form a capacitor cell. The conductive sides of both slides faced inward and were overlaid using a U-shaped 0.5 mm-thick silicone rubber spacer (Altec) creating a chamber. The chamber is filled with the degassed 300 mM sucrose (Sigma-Aldrich) solution in Milli-Q water and sealed using plastic paraffin film (Parafilm) and paper clips. Electroformation is then carried out using a function generator. A 10 Hz sinusoidal potential with a 1 V peak-to-peak amplitude is applied across the chamber for 2 h, after which the frequency is reduced to 2 Hz for 1 h. The vesicles are extracted from the chamber using a pipette and stored in a vial (Eppendorf) at room temperature in the dark. The GUVs obtained are used within 7 days.

2.3. SLB Preparation. Small unilamellar vesicles (SUVs), used to form SLBs, are prepared according to the protocol in ref 16. Briefly, 200 μ L of a 25 mg mL⁻¹ chloroform solution of DOPC + Oregon Green DHPE (99.3:0.7 molar ratio) is injected into a glass vial and desiccated for 15 min to let the chloroform evaporate. The dried lipids are then resuspended in 500 μ L of 300 mM sucrose solution in water and vortexed to ensure hydration. Four freeze/thaw cycles are then carried out using liquid nitrogen and warm water to break apart large lipid structures. To prepare SUVs, the lipid solution is processed using a Mini-Extruder kit (Avanti Polar Lipids) equipped with a track-etched polycarbonate membrane with 0.1 μ m pores (Whatman) and operated according to the manufacturer's instructions. The SUVs are then stored at 4 °C and used within 7 days.

Experimental chambers are prepared by adhering silicone rubber multiwell plates (each well measuring 6.5 \times 6.5 \times 3.2 mm³; Sigma-Aldrich) onto microscope coverslips (24 \times 60 mm², no. 1, Menzel-Glaser), previously cleaned according to the protocol in ref 41. The surface of the coverslip is hydrophilized by plasma cleaning (Femto, Diener Electronic), at a frequency of 40 kHz, pressure of 30 Pa, and power input of 100 W for 5 min. Each chamber is then immediately filled with 100 μ L of an SUV solution obtained by diluting the extruded samples in a ratio of 1:9 in a solution containing 5 mM MgCl₂ and 272 mM glucose in Tris-EDTA (TE) buffer. The contents of the chambers are incubated for 30 min at room temperature to form a defect-free supported bilayer from the rupture of SUVs onto the hydrophilic glass. Excess lipids and magnesium are then removed from the chambers by two rinses with the buffer used in the experiment (hereafter indicated as "experimental buffer", TE + 100 mM NaCl + 87 mM glucose). The chambers are then filled with a known amount of experimental buffer, 110 μ L below the overall capacity of the wells. The formed SLBs are then inspected under a confocal microscope to check for uniform fluorescence and used immediately for sample preparation (see section 2.5).

2.4. DNA Preparation. Double-stranded DNA tethers are assembled from two complementary 33-nucleotide-long single-stranded (ss)DNA molecules purchased lyophilized from Integrated DNA Technology. One of the DNA strands is functionalized with a cholesterol molecule at its 3' end via a TEG linker, whereas the other has a biotin on its 3' end. These are reconstituted in TE buffer (Sigma-Aldrich), aliquoted, and stored at -20 °C. Equal amounts of each single strand are diluted to 1.6 μ M in TE buffer containing 100 mM NaCl. To help hybridization, the solution is heated up to 90 °C and then slowly cooled down on a PCR machine (Eppendorf Master-Cycler). The sequences of the two (ss)DNA strands are (i) 5'-CGT GCG CTG GCG TCT GAA AGT CGA TTG CGA AAA-3'-cholesterol-TEG and (ii) 5'-CGC AAT CGA CTT TCA GAC GCC AGC GCA CGA AAA-3'-biotin. To improve flexibility, single-stranded A₄ spacers are included between the duplex and the functional groups.

2.5. Sample Preparation. The experimental chambers prepared as described in section 2.3 are filled with 90 μ L of experimental buffer containing 22.2 nM of the previously hybridized DNA constructs (see section 2.4), immediately followed by 10 μ L of the GUV solution (see section 2.2), previously diluted down to 1:19 in 300 mM glucose solution. The DNA is expected to uniformly partition on the SLB and the GUVs. We estimate a surface density of receptors of $\rho_R = 2.3 \times 10^4 \mu\text{m}^{-2}$.

We prepare solutions at different concentrations c_{SA} of SA—Alexa Fluor 647 (Thermo Fisher) in experimental buffer and add 10 μ L to the wells before carefully mixing using a pipette, sealing with a Flexwell Seal Strip (Grace Bio-Labs), and incubating for 1 h. The final bulk concentration of DNA receptors in the chamber is $c_{DNA} = c_0 = 18.2$ nM. The stoichiometric ratio used as the control parameter is calculated as $\chi = c_{SA}/c_0$ and ranges between 8×10^{-6} and 80. The final osmolarity of the solutions outside and inside of the GUVs is equal to 300 mM, resulting in osmolarity-matched samples.

2.6. Imaging and Image Analysis. Imaging is carried out on a Leica TCS SP5 II laser-scanning confocal microscope equipped with a Leica HXC PL APO CS 63 \times 1.4 NA oil-immersion objective. A 633 nm He-Ne laser and a 488 argon-ion laser are used to excite, respectively, Alexa 647 labeling the SA molecules and Oregon Green labeling the membranes. Emission is obtained between 497 and 600 nm for the Oregon Green and 639 and 780 nm for the Alexa 647 channels.

A customized script written in MatLab is used for image analysis. Morphological changes in the vesicle are assessed by taking confocal Z-stacks from below the SLB to above the vesicle. Figure 1b shows 3D reconstructions obtained from typical Z-stacks using the 3D Viewer plugin of ImageJ.⁴² The SLB plane is determined as the Z-slice with the maximum average intensity on the He-Ne channel. The presence/absence of a stable patch is determined visually. For vesicles displaying a bright adhesion patch, a Gaussian filter is applied to remove the pixel-level noise. Thresholding is then used to reconstruct the patch. From the area of the patch, the patch radius R_p is derived (see Figure 1). We measure the equatorial radius R (see Figure 1) of the vesicle by analyzing the Z-stack recorded on the Oregon Green channel. A circle is fitted to the vesicle contour for each Z-slice above the SLB plane. The frame with the largest circle is defined as the equatorial plane; from this, the equatorial radius R is measured. The contact angle is then calculated as $\theta = \arcsin(R_p/R)$.

Whenever a patch is present, we also determine from the SLB plane the ratio I between the average fluorescence intensities measured within and outside of the patch. This ratio, measured on the Alexa 647 channel, is used to determine the ratio between the concentration of SA attached to the free-standing SLB and that present on the GUV-SLB contact region.

2.7. Flickering Spectroscopy. We use flickering spectroscopy⁴³⁻⁴⁵ to assess membrane tension in adhering and non-adhering GUVs. Videos of the equator of GUVs are recorded on the Oregon Green channel, as described in ref 16. The time evolution of the vesicle contour is determined from the videos with subpixel resolution using a customized MatLab algorithm, and the mean-squared amplitude of the power spectrum is calculated $\langle |h^2(q_n)| \rangle$, where $q_n = (2\pi/l)n$ ($n = 1, 2, 3, \dots$) is the wave vector along the equatorial contour of length l .¹⁶ The power spectrum amplitude can then be fitted to an established model to extract membrane tension σ (eq 11 of Pécrciaux et al.⁴⁴). Adhering vesicles have much higher tension than non-adhering ones,¹⁶ reducing the amplitude and correlation time of the fluctuations.⁴⁴ Owing to the limited spatiotemporal resolution of our instrument, we are unable to assess $\langle |h^2(q_n)| \rangle$ within a sufficiently broad range of q_n for the fitting to be reliable. Thus, for adhering vesicles, we use the squared amplitude of the low- q equatorial mode 3 as a qualitative indicator for membrane tension. Mode $q = 3$ is chosen as the lowest- q mode carrying unbiased information on the membrane tension, mode $n = 1$ being associated to vesicle translation and mode $n = 2$ being heavily biased by imaging artifacts.

2.8. FRAP. FRAP is carried out to determine binding/unbinding kinetics of intermembrane bonds using the dedicated Leica software.

We consider adhering GUVs, and after imaging the adhesion area on the SLB plane for 10 s, we bleach the SA molecules within the adhesion patch by exposing it to high-intensity excitation light for 9.7 s. We then monitor the fluorescence recovery of the bleached area for 1235 s. For the first 10 s, we image at 10 fps, thereafter at 0.5 fps for 4 min, and subsequently at 0.1 fps. The ratio $I(t)$ between fluorescence intensities measured within and outside of the adhesion patch is measured as a function of time, as described in section 2.6, with $t = 0$ corresponding to the first frame taken after bleaching. The recovery in $I(t)$ carries information on loop-like complexes and passivated receptors rapidly diffusing in and out of the adhesion patch as well as bridge-like complexes that require unbinding events to leave the adhesion area (see Figure 1a).

3. MODELING SA/DNA COMPLEXATION

Much of the phenomenology discussed in the remainder of this article arises from the possibility of each SA ligand to bind between one and four biotin–DNA receptors. We indicate the resultant multimeric complexes as *monomers*, *dimers*, *trimers*, and *tetramers*, as sketched in Figure 1a. Given their strong affinity, it is safe to model SA/biotin linkages as irreversible, meaning that the fraction of ligands involved in each of the multimeric complexes is fixed at the moment of sample preparation and remains unchanged throughout the experiment. In turn, as discussed in section 2.8 measurements of bond reversibility, cholesterol anchors can detach from the bilayers, enabling equilibration of the populations of loop-like and bridge-like complexes over accessible time scales (Figure 1a).

We label the total bulk concentration of DNA receptors and SA as $c_{\text{DNA}} = c_0$ and $c_{\text{SA}} = \chi c_0$, whereas $c_{1,k}$ (with $k = 1, \dots, 4$) denotes the concentrations of complexes made by k DNA strands binding SA (see Figure 1a). For a given stoichiometric ratio χ , $c_{1,k}$ can be calculated using equilibrium chemical reactions

$$c_{1,k} = Kc_{1,k-1}c_{0,1} \quad k \in [1, 4] \quad (1)$$

where $c_{0,1}$ and $c_{1,0}$ are the concentrations of unbound DNA and SA, and K is the association kinetic constant of the SA–biotin complex (in this work $K \rightarrow \infty$). Conservation of the total number of DNA and SA molecules implies

$$\begin{aligned} c_0 &= c_{0,1} + c_{1,1} + 2c_{1,2} + 3c_{1,3} + 4c_{1,4} \\ c_0\chi &= c_{1,0} + c_{1,1} + c_{1,2} + c_{1,3} + c_{1,4} \end{aligned} \quad (2)$$

Two concentration regimes can be identified: $\chi > 1/4$ and $\chi \leq 1/4$.

$\chi > 1/4$. Because the association between DNA and SA is maximized ($K \rightarrow \infty$ in eq 1), at high χ , no unbound DNA is left in solution ($c_{0,1} = 0$) whereas free SA is present ($c_{1,0} > 0$). From eq 1, taking $Kc_{0,1}$ as constant, we obtain

$$\alpha = \frac{c_{1,4}}{c_{1,3}} = \frac{c_{1,3}}{c_{1,2}} = \frac{c_{1,2}}{c_{1,1}} = \frac{c_{1,1}}{c_{1,0}} \quad (3)$$

and using eq 2 with $c_{0,1} = 0$ we obtain

$$c_{1,0} = \frac{c_0}{\alpha + 2\alpha^2 + 3\alpha^3 + 4\alpha^4} \quad (4)$$

$$\chi = \frac{1 + \alpha + \alpha^2 + \alpha^3 + \alpha^4}{\alpha + 2\alpha^2 + 3\alpha^3 + 4\alpha^4} \quad (5)$$

Equation 5 admits a unique solution for α that can be used to calculate $c_{1,0}$ first (see eq 4) and then $c_{1,k}$ using eq 3 and the value of $c_{1,0}$.

$\chi \leq 1/4$. When $\chi = 1/4$, only tetramers are present in solution ($c_{1,4} = \chi c_0$), whereas $c_{1,0} = 0$. For $\chi \leq 1/4$, the amount of SA is not sufficient to bind all available receptor strands, resulting in a finite concentration of free DNA, $c_{0,1} = c_0(1 - 4\chi)$.

Figure 2a summarizes the concentration of all possible complexes as a function of χ normalized by the total

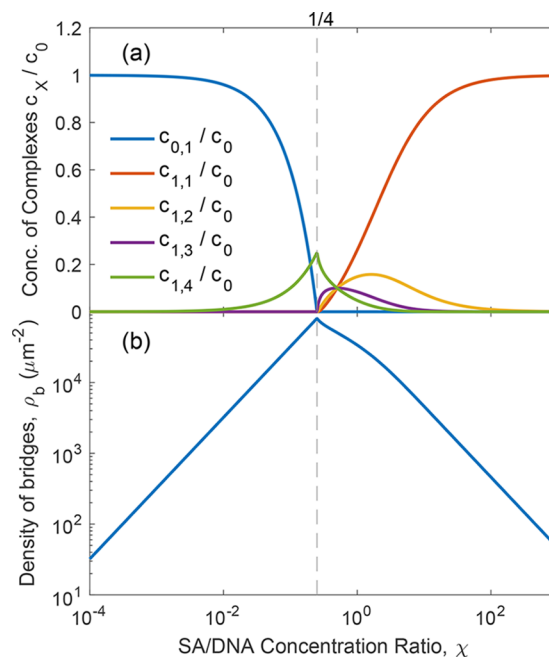


Figure 2. Modeling distribution of multimeric complexes. (a) Fraction of receptors involved in different complexes with SA ligands as a function of the relative ligand concentration χ . For $\chi \leq 1/4$, only tetramers are present. Trimers, dimers, and monomers appear for $\chi > 1/4$. If the SA concentration is further increased, the majority of the receptors are passivated by a single ligand. (b) Surface density of bridge-like complexes ρ_b as a function of χ . ρ_b peaks at $\chi = 1/4$ and drops upon increasing or decreasing the SA concentration, compatible with the observation on GUV adhesion (see Figure 3b).

concentration of DNA c_0 . At high χ , only *passivated* receptors, bound to a single SA ligand (monomers), are present. Therefore, $c_{1,1} \approx c_0$ and $c_{1,2,\dots,4} \approx c_{1,0} \approx 0$. When decreasing χ , higher-order complexes become available: first dimers, then trimers, and tetramers. On further lowering χ , the excess of receptors suppresses the formation of dimers and trimers, and for $\chi \leq 1/4$, only tetramers are present, coexisting with free receptors.

Assuming that the biotin–SA association happens much faster than cholesterol adsorption into the lipid bilayers, we now estimate the concentration of bridge-like complexes within the patch area. We neglect the interactions between different complexes and calculate the probability of finding a complex in the patch area given the concentration of the same complex on the lipid bilayer outside of the patch area, which is modeled as an infinite reservoir. The surface densities ρ_X ($X = \{1, 0\}$, $\{0, 1\}$, $\{1, k\}$, $k = [1, 4]$) are proportional to the bulk concentration, that is, $\rho_X = a \cdot c_X$, with a that does not depend on the type of complex. Neglecting the surface area of the GUVs as compared with that of the SLB, which is much larger,

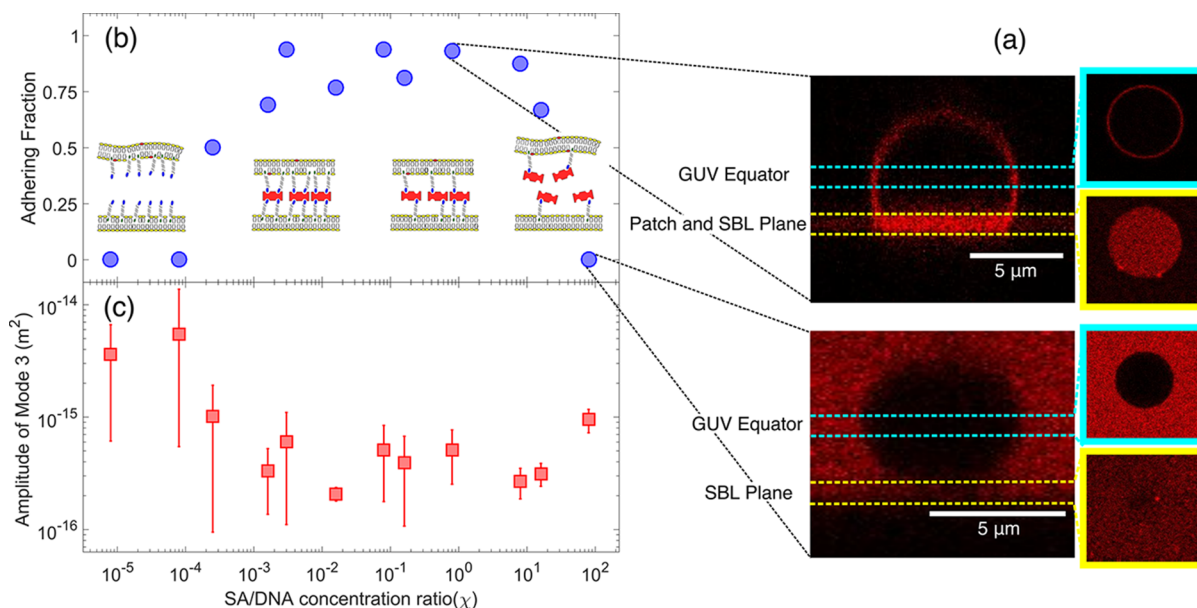


Figure 3. Quantifying GUV adhesion and induced membrane tension. (a) Confocal cross section, equatorial section, and SLB plane in an adhering GUV (left, $\chi = 8 \times 10^{-1}$) and a non-adhering GUV (right, $\chi = 8 \times 10^1$). (b) Fraction of adhering GUVs as a function of the relative ligand concentration χ , as determined by visual inspection in samples averaging 14 GUVs (for each value of χ). The insets sketch the architecture of complexes expectedly present within the adhesion patch. Adhesion is observed within an *intermediate* range of concentrations where the surface density of bridges is sufficiently high (see Figure 2b). (c) Mean-squared amplitude of equatorial fluctuation mode $n = 3$ as measured using flickering spectroscopy. The amplitude drop in the intermediate regime corresponds to an increase in the membrane tension induced by adhesion. Experimental points and error bars are calculated as the mean and standard deviation in samples averaging 12 GUVs (for each value of χ).

and assuming that all of the receptors partition on a lipid membrane,⁴⁶ we estimate $a \approx 2.1 \times 10^3 \mu\text{m}^{-2} \text{nM}^{-1}$. Although this is strictly true only if all of the cholesterol anchors absorb onto the bilayer, this should be the case given the dissociation constant of 17 nM.

The complexes found within the patch area can have either a loop-like or a bridge-like character, as sketched in Figure 1a. We assume that configurational costs of adsorbing a complex in loop-like or bridge-like configurations are equal. Our recent finding suggests that this is the case for distances between the GUV patch and the SLB comparable with DNA strand length.^{16–18} In particular, this assumption is also justified by the configurational freedom enabled by the use of freely rotating dsDNA spacers. Because the pairs of binding sites are arranged on opposite sides of the SA molecules, if biotin receptors were directly grafted to the lipids,^{32,33} the formation of loops with tetrameric complexes would be highly hindered. However, because dsDNA spacers ($L \approx 10$ nm) are longer than the diameter of SA (~ 5 nm), and cholesterol and biotin are connected through flexible spacers made of four unpaired bases, all possible binding configurations are geometrically accessible.

Each complex of type $\{1, k\}$ in the patch region has 2^k possible ways of arranging the k DNA “arms” between the two bilayers. Out of these, two configurations are loop-like and the remaining $2k - 2$ configurations are bridge-like. It follows that dimers ($k = 2$) have equal chances of forming loops or bridges, but trimers ($k = 3$) and tetramers ($k = 4$) are more likely to form bridges than loops by a factor of 3 and 7, respectively.

In Figure 2b, we therefore show the surface density of bridge-like complexes within the patch, calculated as $\rho_b = a \sum_{k=1}^4 (2^k - 2) c_{1,k}$. We observe a region of intermediate SA concentrations with a high density of bridges that peaks at $\chi = 1/4$.

4. RESULTS AND DISCUSSION

4.1. Morphological Response to Ligand Concentration.

The 3D reconstructions from confocal Z-stacks, shown in Figure 1 as recorded on the Oregon Green (lipid) channel, exemplify the morphological difference between an adhering vesicle having the shape of a truncated sphere (Figure 1b) and a more spherical non-adhering one (Figure 1c). The clear shape difference enables us to distinguish easily between adhering and non-adhering vesicles, as also demonstrated in Figure 3a, where we show vertical confocal sections of the GUVs, the equatorial cross sections, and the SLB plane, all recorded on the SA (Alexa 647) fluorescence channel. Figure 3b shows the observed fraction of adhering GUVs as a function of the bulk concentration ratio between the SA ligands and receptors (χ).

Three regimes can be clearly identified: *low* ($\chi \lesssim 3 \times 10^{-4}$), *intermediate* ($3 \times 10^{-3} \lesssim \chi \lesssim 20$), and *high* ($\chi \gtrsim 20$) SA concentrations. The theoretical estimate made in section 3 indicates that in the low ligand concentration regime, all of the SA receptors give rise to tetrameric complexes, but the number of bridges formed between the GUV and the SLB is still too low to cause the formation of a stable adhesion patch (see Figure 2b). Within the broad range of intermediate SA concentrations, a stable adhesion patch is observed for the majority of the GUVs. Here, the confocal lateral and equatorial sections demonstrate the presence of SA molecules on the GUV and SLB membranes. Adhesion sets in already at $\chi \approx 3 \times 10^{-4}$, where only a small fraction of the receptors are bound to ligands. However, most of the receptors form tetrameric complexes with high chances of bridge formation, resulting in a sufficiently high number of GUV–SLB bonds (see Figure 2b). The strong tendency toward the bridge formation of tetrameric complexes also produces a significant accumulation of SA within the adhesion patch, as compared with non-adhering areas of the SLB and GUV. Indeed, the ratio between Alexa 647

fluorescence intensity measured within and outside of the patch at $\chi = 8 \times 10^{-4}$ is $\bar{I} = 16.7 \pm 8.1$. When the number of SA molecules exceeds one-fourth of that of the DNA receptors, all of the binding sites are saturated, and some of the SA ligands are bound to three or fewer receptors. As we approach the high-concentration regime, for $\chi = 8$, the SA fluorescence intensity ratio between the adhesion patch and the free SLB drops to $\bar{I} = 2.18 \pm 0.33$. Here, most of the DNA receptors are passivated by single SA and therefore uniformly distributed across the membranes within and outside of the patch, hence explaining the intensity ratio approaching the limit of noninteracting membranes (i.e., 2). Only a small number of ligands are involved in multimeric complexes stabilizing the patch. For $\chi \gtrsim 20$, we enter the high-concentration regime, where nearly all SA are either free in solution or tethered to a single receptor, and the number of multimeric SA complexes is too low for a stable adhesion. Confocal lateral and equatorial sections confirm that in the high-concentration regime, most of the SA molecules remain free in solution (Figure 3a).

4.2. Mechanical Response: Membrane Tension. Figure 3c shows the mean-squared amplitude $\langle |h^2(q_3)| \rangle$ of equatorial fluctuation mode $n = 3$ as a function of χ . In the high-tension limit, the rough proportionality $1/\sigma \propto \langle |h^2(q_3)| \rangle$ holds, which, however, cannot be used to quantitatively extract σ .⁴⁴ Nonetheless, the three adhesion regimes are clearly reflected in $\langle |h^2(q_3)| \rangle$. In the low-SA-concentration regime, non-adhering vesicles display $\langle |h^2(q_3)| \rangle \approx 10^{-14}$ to 10^{-15} m². In the intermediate regime, from the onset of adhesion, we observe a drop in the fluctuation amplitude, with $\langle |h^2(q_3)| \rangle$ decreasing by approximately 1 order of magnitude. As we approach the high-SA-concentration regime, the lack of adhesion causes an increase in the fluctuation amplitude.

The sharp changes in tension at the boundaries between the three regimes demonstrate the correlation between the GUV morphology, that is, patch formation, and the mechanical properties of the membranes.

Although, as explained in section 2.7, the membrane tension σ cannot be reliably measured within the intermediate regime, in the low- and high-SA-concentration regimes, an accurate estimate can be made by fitting $\langle |h^2(q_n)| \rangle$. At $\chi = 8 \times 10^{-6}$, we obtain $\sigma = 1.8 \pm 0.5 \times 10^{-6}$ Nm. The large error bar is partially a consequence of the broad distribution of excess areas typical of electroformed liposomes. In adhering vesicles, differences in excess area result in changes in the size of the adhesion patch, which has a smaller influence on the membrane tension.¹⁶

4.3. FRAP Measurements of Bond Reversibility. Figure 4a shows a sequence of confocal images of an adhesion patch as taken in the Alexa 647 (SA) channel over a typical FRAP experiment. Before the bleaching step, a clearly defined bright patch is visible, with a patch/SLB intensity ratio equal to \bar{I}_{PB} . Exposure of the adhesion area to high-intensity excitation causes an almost complete bleaching of the SA molecules. Recovery is then monitored over time using the patch/SLB intensity ratio $\bar{I}(t)$.

The adhesion patch is populated by both loop-like and bridge-like complexes (see Figure 1a). The former, together with passivated receptors, can freely move in and out of the patch area through lateral diffusion on either SLB or GUV membranes, resulting in a quick recovery of part of the fluorescence signal. In turn, the bridge-like complexes are confined within the patch area, being able to leave only upon bond breakup. Full recovery of the fluorescence signal therefore

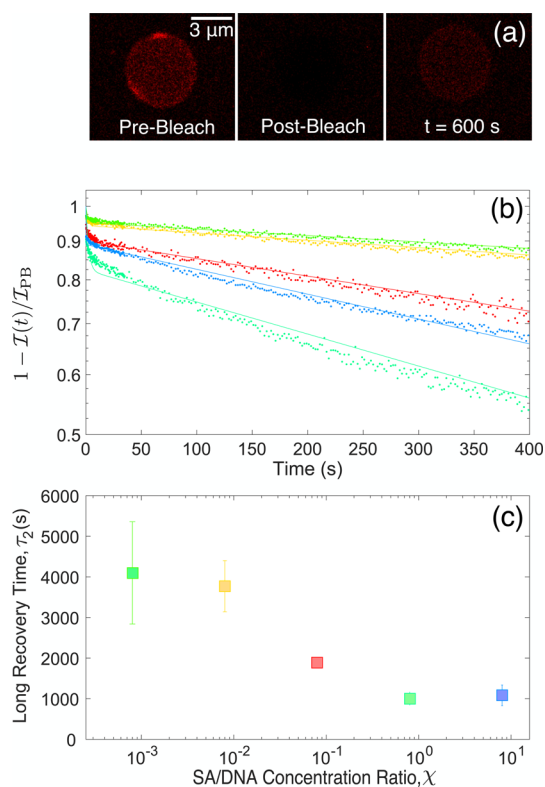


Figure 4. FRAP measurements of bridge unbinding kinetics. (a) Sequence of images of the adhesion patch before the SA molecules are bleached (left), immediately after bleaching (middle), and after partial recovery of the fluorescence intensity has occurred (right). (b) Fluorescence recovery profiles: $1 - I(t) / I_{PB}$. Solid lines are best fits using eq 6. (c) Slow-recovery time constant τ_2 (see eq 6) as a function of relative SA concentration χ . Experimental points and error bars are calculated as the mean and standard deviation in samples averaging 6 GUVs (for each value of χ).

occurs on timescales dependent on the breakup of GUV–SLB bonds. In view of these two timescales, we fit the patch/SLB intensity ratio $\bar{I}(t)$ with a double exponential

$$1 - \frac{\bar{I}(t)}{I_{PB}} = A \exp\left(-\frac{t}{\tau_1}\right) + (1 - A) \exp\left(-\frac{t}{\tau_2}\right) \quad (6)$$

where τ_1 is the fast recovery time associated with the diffusion of loop-like complexes and passivated receptors, τ_2 ($> \tau_1$) is the slow recovery time associated with bridge breakup, and A is a parameter quantifying the fraction of the initial fluorescence intensity undergoing fast recovery.

Figure 4b shows recovery curves collected at different χ values and fitted with eq 6, whereas Figure 4c summarizes the dependency of τ_2 on χ . Two processes could be involved in the bridge breakups leading to the full recovery of the signal: the breakup of biotin/SA bonds or the yielding of the connection between the cholesterol anchor and the lipid bilayers. The off-rate of biotin/SA bonds, as estimated according to the parametric formula of Koussa et al.,⁴⁷ is $k_{off} = 6.3 \times 10^{-7}$ s⁻¹. The off-rate of the bond between a cholesterol-tethered DNA molecule and an SLB, as evaluated by Pfeiffer and Höök,⁴⁶ $k_{off} = 5.8 \times 10^{-4}$ s⁻¹, is much higher and is compatible with the recovery timescales we measure. We can therefore deduce that the process responsible for bond rearrangement in our systems

is the thermal extraction of cholesterol anchors from the lipid bilayers.

Figure 4b demonstrates a drop in τ_2 as χ increases within the intermediate-SA-concentration regime. This behavior can once again be qualitatively explained by the χ dependence of the valence of multimeric complexes. For $\chi \leq 1/4$, ligands form only tetrameric complexes and, as discussed in section 3, seven out of eight tetramers are in a bridge-like configuration. Four of these seven tetramers have three receptors anchored to one membrane and one receptor anchored to the other, whereas the remaining three tetramers have two receptors on each membrane. The latter complexes, therefore, need to break and re-form at least two bonds to turn into loop-like complexes and diffuse out of the membrane, resulting in a slow fluorescence recovery. As χ is increased above 1/4, a fraction of the bridge-like complexes turn out to be trimers or dimers, which can exit the adhesion patch by breaking and re-forming only one bond; hence, the fluorescence recovery is faster.

5. CONCLUSIONS

We have studied the morphological and mechanical responses in single giant liposomes adhering to a flat supported lipid bilayer, caused by changes in the concentration of the ligand molecules mediating the attraction. Biotin-functionalized DNA receptors are tethered to the membranes through a cholesterol anchor. SA ligands dispersed in solution bind the receptors, forming multimeric complexes that feature one to four receptors per ligand. The complexes can either take a loop-like arrangement, when all of the bound receptors are anchored to the same membrane, or take a bridge-like arrangement between the GUVs and the SLB.

For a fixed concentration of ligands, we observe stable adhesion only when the concentration of SA receptors falls within a well-defined range. Adhering vesicles display a large increase in membrane tension. We find an accumulation of SA receptors within the adhesion patch as compared with the concentration of those tethered to free membranes, which becomes less pronounced at higher SA concentrations. The unbinding kinetics of intermembrane bridges, caused by the reversibility of cholesterol insertion, is probed via FRAP. The average unbinding rate of bridges is lower at low SA concentrations.

The observed phenomenology can be rationalized using a simple model that accounts for the tetravalent nature of SA–biotin complexes. Re-entrant unbinding upon increasing the linker concentration is a general phenomenon recently observed in the context of nanoparticle self-assembly.⁴⁸ Here, the effect is rationalized for the case of diffusive multimeric linkers, but a general discussion of the problem will follow in a dedicated contribution.

We argue that the sharp onset of vesicle adhesion could be exploited to build (bio)molecular sensing devices, the purpose of which would be to sense the presence of an analyte above a certain concentration threshold that triggers membrane adhesion and changes in shape and tension of the vesicles. The detection threshold can potentially be tuned by including synthetic linkers (e.g., made up of DNA) forming a small number of permanent bridges, enough to bring the membranes very close to the onset of adhesion. From there, a very small amount of the target ligand would trigger adhesion and therefore be detected. Readouts can be generated optically or via impedance measurements using microfluidic devices featuring integrated electrodes.

Furthermore, the findings presented here are relevant to the study of multivalent interactions in adhesion between cells, in particular those dependent on linker molecules such as cadherins and selectins.⁴⁹

AUTHOR INFORMATION

Corresponding Authors

*E-mail: ld389@cam.ac.uk (L.D.M.).

*E-mail: pc245@cam.ac.uk (P.C.).

ORCID

Bortolo M. Moggetti: 0000-0002-7960-8224

Pietro Cicuta: 0000-0002-9193-8496

Lorenzo Di Michele: 0000-0002-1458-9747

Notes

The authors declare no competing financial interest.

A complete dataset in support of this publication is available free of charge at <https://doi.org/10.17863/CAM.6919>.

ACKNOWLEDGMENTS

O.A.A. acknowledges support from the EPSRC Centre for Doctoral Training in Sensor Technology and Applications, Grant number EP/L015889/1. O.A.A., P.C., and L.D.M. acknowledge support from the EPSRC Programme Grant CAPITALS number EP/J017566/1. L.D.M. acknowledges support from the Oppenheimer Fund, Emmanuel College Cambridge, and The Leverhulme Trust through an Early Career Research Fellowship underwritten by the Isaac Newton Trust. B.M.M. acknowledges support from the Université Libre de Bruxelles (ULB). The authors thank L. Parolini for discussion and support with vesicle preparation and both her and D. Orsi for help with the flickering analysis software.

REFERENCES

- (1) Michele, L. D.; Eiser, E. Developments in understanding and controlling self assembly of DNA-functionalized colloids. *Phys. Chem. Chem. Phys.* **2013**, *15*, 3115–3129.
- (2) Hill, H. D.; Macfarlane, R. J.; Senesi, A. J.; Lee, B.; Park, S. Y.; Mirkin, C. A. Controlling the lattice parameters of gold nanoparticle FCC crystals with duplex DNA linkers. *Nano Lett.* **2008**, *8*, 2341–2344.
- (3) Nykypanchuk, D.; Maye, M. M.; van der Lelie, D.; Gang, O. DNA-guided crystallization of colloidal nanoparticles. *Nature* **2008**, *451*, 549–552.
- (4) Park, S. Y.; Lytton-Jean, A. K. R.; Lee, B.; Weigand, S.; Schatz, G. C.; Mirkin, C. A. DNA-programmable nanoparticle crystallization. *Nature* **2008**, *451*, 553–556.
- (5) Macfarlane, R. J.; Lee, B.; Jones, M. R.; Harris, N.; Schatz, G. C.; Mirkin, C. A. Nanoparticle Superlattice Engineering with DNA. *Science* **2011**, *334*, 204–208.
- (6) Mirkin, C. A.; Letsinger, R. L.; Mucic, R. C.; Storhoff, J. J. A DNA-based method for rationally assembling nanoparticles into macroscopic materials. *Nature* **1996**, *382*, 607–609.
- (7) Alivisatos, A. P.; Johnsson, K. P.; Peng, X.; Wilson, T. E.; Loweth, C. J.; Bruchez, M. P.; Schultz, P. G. Organization of “nanocrystal molecules” using DNA. *Nature* **1996**, *382*, 609–611.
- (8) Thaxton, C. S.; Elghanian, R.; Thomas, A. D.; Stoeva, S. I.; Lee, J.-S.; Smith, N. D.; Schaeffer, A. J.; Klocker, H.; Horninger, W.; Bartsch, G.; Mirkin, C. A. Nanoparticle-based bio-barcode assay redefines “undetectable” PSA and biochemical recurrence after radical prostatectomy. *Proc. Natl. Acad. Sci. U.S.A.* **2009**, *106*, 18437–18442.
- (9) Young, K. L.; Ross, M. B.; Blaber, M. G.; Rycenga, M.; Jones, M. R.; Zhang, C.; Senesi, A. J.; Lee, B.; Schatz, G. C.; Mirkin, C. A. Using DNA to design plasmonic metamaterials with tunable optical properties. *Adv. Mater.* **2014**, *26*, 653–659.

- (10) Leunissen, M. E.; Dreyfus, R.; Sha, R.; Wang, T.; Seeman, N. C.; Pine, D. J.; Chaikin, P. M. Towards self-replicating materials of DNA-functionalized colloids. *Soft Matter* **2009**, *5*, 2422.
- (11) Maye, M. M.; Kumara, M. T.; Nykypanchuk, D.; Sherman, W. B.; Gang, O. Switching binary states of nanoparticle superlattices and dimer clusters by DNA strands. *Nat. Nanotechnol.* **2010**, *5*, 116–120.
- (12) Tison, C. K.; Milam, V. T. Reversing DNA-mediated adhesion at a fixed temperature. *Langmuir* **2007**, *23*, 9728–9736.
- (13) Rogers, W. B.; Manoharan, V. N. Programming colloidal phase transitions with DNA strand displacement. *Science* **2015**, *347*, 639–642.
- (14) Pontani, L.-L.; Jorjadze, I.; Viasnoff, V.; Brujic, J. Biomimetic emulsions reveal the effect of mechanical forces on cell–cell adhesion. *Proc. Natl. Acad. Sci. U.S.A.* **2012**, *109*, 9839–9844.
- (15) van der Meulen, S. A. J.; Leunissen, M. E. Solid colloids with surface-mobile DNA linkers. *J. Am. Chem. Soc.* **2013**, *135*, 15129–15134.
- (16) Shimobayashi, S. F.; Mognetti, B. M.; Parolini, L.; Orsi, D.; Cicuta, P.; Di Michele, L. Direct measurement of DNA-mediated adhesion between lipid bilayers. *Phys. Chem. Chem. Phys.* **2015**, *17*, 15615–15628.
- (17) Parolini, L.; Mognetti, B. M.; Kotar, J.; Eiser, E.; Cicuta, P.; Di Michele, L. Volume and porosity thermal regulation in lipid mesophases by coupling mobile ligands to soft membranes. *Nat. Commun.* **2015**, *6*, 5948.
- (18) Parolini, L.; Kotar, J.; Di Michele, L.; Mognetti, B. M. Controlling self-assembly kinetics of DNA-functionalized liposomes using toehold exchange mechanism. *ACS Nano* **2016**, *10*, 2392–2398.
- (19) Beales, P. A.; Vanderlick, T. K. Application of nucleic acid–lipid conjugates for the programmable organisation of liposomal modules. *Adv. Colloid Interface Sci.* **2014**, *207*, 290–305.
- (20) Beales, P. A.; Nam, J.; Vanderlick, T. K. Specific adhesion between DNA-functionalized “Janus” vesicles: Size-limited clusters. *Soft Matter* **2011**, *7*, 1747–1755.
- (21) Beales, P. A.; Vanderlick, T. K. Specific Binding of Different Vesicle Populations by the Hybridization of Membrane-Anchored DNA. *J. Phys. Chem. A* **2007**, *111*, 12372–12380.
- (22) Hadorn, M.; Boenzli, E.; Sørensen, K. T.; De Luca, D.; Hanczyc, M. M.; Yomo, T. Defined DNA-mediated assemblies of gene-expressing giant unilamellar vesicles. *Langmuir* **2013**, *29*, 15309–15319.
- (23) Hadorn, M.; Boenzli, E.; Sørensen, K. T.; Fellermann, H.; Hotz, P. E.; Hanczyc, M. M. Specific and reversible DNA-directed self-assembly of oil-in-water emulsion droplets. *Proc. Natl. Acad. Sci. U.S.A.* **2012**, *109*, 20320–20325.
- (24) Hadorn, M.; Hotz, P. E. DNA-Mediated Self-Assembly of Artificial Vesicles. *PLoS One* **2010**, *5*, e9886.
- (25) Langowska, K.; Palivan, C. G.; Meier, W. Polymer nanoreactors shown to produce and release antibiotics locally. *Chem. Commun.* **2012**, 128–130.
- (26) Noireaux, V.; Maeda, Y. T.; Libchaber, A. Development of an artificial cell, from self-organization to computation and self-reproduction. *Proc. Natl. Acad. Sci. U.S.A.* **2011**, *108*, 3473–3480.
- (27) Peters, R. J. R. W.; Louzao, I.; van Hest, J. C. M. From polymeric nanoreactors to artificial organelles. *Chem. Sci.* **2012**, *3*, 335.
- (28) Chan, Y.-H. M.; van Lengerich, B.; Boxer, S. G. Lipid-anchored DNA mediates vesicle fusion as observed by lipid and content mixing. *Biointerphases* **2008**, *3*, FA17–FA21.
- (29) Chan, Y.-H. M.; van Lengerich, B.; Boxer, S. G. Effects of linker sequences on vesicle fusion mediated by lipid-anchored DNA oligonucleotides. *Proc. Natl. Acad. Sci. U.S.A.* **2009**, *106*, 979–984.
- (30) Parolini, L.; Kotar, J.; Di Michele, L.; Mognetti, B. M. Controlling Self-Assembly Kinetics of DNA-Functionalized Liposomes Using Toehold Exchange Mechanism. *ACS Nano* **2016**, *10*, 2392–2398.
- (31) Di Michele, L.; Bachmann, S. J.; Parolini, L.; Mognetti, B. M. Communication: Free energy of ligand–receptor systems forming multimeric complexes. *J. Chem. Phys.* **2016**, *144*, 161104.
- (32) Chiruvolu, S.; Walker, S.; Israelachvili, J.; Schmitt, F. J.; Leckband, D.; Zasadzinski, J. A. Higher order self-assembly of vesicles by site-specific binding. *Science* **1994**, *264*, 1753–1756.
- (33) Walker, S. A.; Kennedy, M. T.; Zasadzinski, J. A. Encapsulation of bilayer vesicles by self-assembly. *Nature* **1997**, *387*, 61–64.
- (34) Bihl, T.; Fenz, S.; Sackmann, E.; Merkel, R.; Seifert, U.; Sengupta, K.; Smith, A.-S. Association Rates of Membrane-Coupled Cell Adhesion Molecules. *Biophys. J.* **2014**, *107*, L33–L36.
- (35) Fenz, S. F.; Merkel, R.; Sengupta, K. Diffusion and Intermembrane Distance: Case Study of Avidin and E-Cadherin Mediated Adhesion. *Langmuir* **2009**, *25*, 1074–1085.
- (36) Fenz, S. F.; Smith, A.-S.; Merkel, R.; Sengupta, K. Intermembrane adhesion mediated by mobile linkers: Effect of receptor shortage. *Soft Matter* **2011**, *7*, 952–962.
- (37) Albersdörfer, A.; Feder, T.; Sackmann, E. Adhesion-Induced Domain Formation by Interplay of Long-Range Repulsion and Short-Range Attraction Force: A Model Membrane Study. *Biophys. J.* **1997**, *73*, 245–257.
- (38) Nam, J.; Santore, M. M. The Adhesion Kinetics of Sticky Vesicles in Tension: The Distinction between Spreading and Receptor Binding. *Langmuir* **2007**, *23*, 10650–10660.
- (39) Noppl-Simson, D. A.; Needham, D. Avidin–Biotin Interactions at Vesicle Surfaces: Adsorption and Binding, Cross-Bridge Formation, and Lateral Interactions. *Biophys. J.* **1996**, *70*, 1391–1401.
- (40) Ratanabankoon, P.; Gropper, M.; Merkel, R.; Sackmann, E.; Gast, A. P. Mechanics of streptavidin-coated giant lipid bilayer vesicles: A micropipet study. *Langmuir* **2003**, *19*, 1054–1062.
- (41) Di Michele, L.; Varrato, F.; Kotar, J.; Nathan, S. H.; Foffi, G.; Eiser, E. Multistep kinetic self-assembly of DNA-coated colloids. *Nat. Commun.* **2013**, *4*, 2007.
- (42) Schmid, B.; Schindelin, J.; Cardona, A.; Longair, M.; Heisenberg, M. A high-level 3D visualization API for Java and ImageJ. *BMC Bioinf.* **2010**, *11*, 274.
- (43) Yoon, Y.-Z.; Hong, H.; Brown, A.; Kim, D. C.; Kang, D. J.; Lew, V. L.; Cicuta, P. Flickering analysis of erythrocyte mechanical properties: Dependence on oxygenation level, cell shape, and hydration level. *Biophys. J.* **2009**, *97*, 1606–1615.
- (44) Pécéréaux, J.; Döbereiner, H.-G.; Prost, J.; Joanny, J.-F.; Bassereau, P. Refined Contour Analysis of Giant Unilamellar Vesicles. *Eur. Phys. J. E: Soft Matter Biol. Phys.* **2004**, *13*, 277–290.
- (45) Helfrich, W.; Servuss, R.-M. Undulations, steric interaction and cohesion of fluid membranes. *Nuovo Cimento D* **1984**, *3*, 137–151.
- (46) Pfeiffer, I.; Höök, F. Bivalent Cholesterol-Based Coupling of Oligonucleotides to Lipid Membrane Assemblies. *J. Am. Chem. Soc.* **2004**, *126*, 10224–10225.
- (47) Koussa, M. A.; Halvorsen, K.; Ward, A.; Wong, W. P. DNA nanoswitches: A quantitative platform for gel-based biomolecular interaction analysis. *Nat. Methods* **2015**, *12*, 123–126.
- (48) Kennedy, Z. C.; Lisowski, C. E.; Mitaru-Berceanu, D. S.; Hutchison, J. E. Influence of Ligand Shell Composition upon Interparticle Interactions in Multifunctional Nanoparticles. *Langmuir* **2015**, *31*, 12742–12752.
- (49) Aplin, A. E.; Howe, A.; Alahari, S. K.; Juliano, R. L. Signal transduction and signal modulation by cell adhesion receptors: The role of integrins, cadherins, immunoglobulin–cell adhesion molecules, and selectins. *Pharmacol. Rev.* **1998**, *50*, 197–263.